ISSN 0026-2617, Microbiology, 2013, Vol. 82, No. 4, pp. 517–524. © Pleiades Publishing, Ltd., 2013.
Original Russian Text © M.V. Zhurina, N.A. Kostrikina, E.Yu. Parshina, E.A. Strelkova, A.I. Yusipovich, G.V. Maksimov, V.K. Plakunov, 2013, published in Mikrobiologiya, 2013, Vol. 82, No. 4, pp. 502–509.

SHORT COMMUNICATIONS

Visualization of the Extracellular Polymeric Matrix of *Chromobacterium violaceum* Biofilms by Microscopic Methods

M. V. Zhurina[a], N. A. Kostrikina[a], E. Yu. Parshina[b], E. A. Strelkova[a], A. I. Yusipovich[b], G. V. Maksimov[b], and V. K. Plakunov[a, 1]

[a] *Winogradsky Institute of Microbiology, Russian Academy of Sciences, pr. 60-letiya Oktyabrya 7, k. 2, Moscow, 117312, Russia*

[b] *Faculty of Biology, Moscow State University, Moscow, Russia*

Received January 9, 2013

DOI: 10.1134/S0026261713040164

We have previously presented results that indicated direct correlation between the ability to form a fully functional matrix and the sensitivity of microbial biofilms to thermal, hyperosmotic, and acidic shock [1]. In particular, we compared the sensitivity to these factors in the pigment-free (producing no violacein) strain *Chromobacterium violaceum* WT, which possesses a normal quorum sensing system and matrix-forming ability, and in the mutant strain *C. violaceum* CV026, with impaired synthesis of *N*-acyl homoserine lactones (AHL), components of the regulatory quorum sensing system, and with a decreased capacity for matrix formation. Violacein synthesis by strain CV026 is induced by *N*-hexanoyl homoserine lactone (C6-AHL), as well as by other AHLs with acyl side chains containing from 4 to 8 carbon atoms. This strain is therefore used as a biosensor for AHLs [2]. In the previously reported experiments [1], biofilm matrix production was quantified according to the standard technique [3] with minor modifications: the matrix was stained with 1,9-dimethylmethylene blue (DMMB) specific to the matrix components, DMMB was extracted with 96% ethanol, and optical density of the extract was measured at 540 nm [1]. Earlier, such dyes as Congo red (staining only cellulose and cellulose-like glycans) [4] and Alcian blue (staining acidic polysaccharides) [5] were proposed to visualize the biofilm matrix. However, the results of the cited work [3], as well as our data (see below) show that DMMB has the highest selectivity toward the matrix components and practically does not stain matrix-free bacterial cells.

The goal of the present work was to test the feasibility of some microscopic methods for visualization of the biofilm matrix and to reveal differences in the process of matrix formation in *C. violaceum* strains under study.

[1] Corresponding author; e-mail: plakunov@inmi.host.ru

For investigation by phase contrast (PCM) and epifluorescence microscopy (EpiFM) (Axio Imager D1 microscope, Carl Zeiss, ×40 lens), laser interference microscopy (LIM), and atomic force microscopy (AFM), the biofilms were formed on cover slips. These slips were sterilized in petri dishes with dry heat. The dishes were filled with 10 mL of sterile LB medium (containing 100 μg/mL kanamycin in the case of the CV026 mutant) and inoculated with 50 μL of 24-h bacterial cultures. The dishes were incubated under stationary conditions at 28–29°C during 48 h. The planktonic culture was removed, the dishes were carefully dried with filter paper, and the biofilms were fixed with delicate heating in a burner flame. For PCM and EpiFM, the biofilms were stained with DMMB according to the standard technique [3] and with DAPI [6], respectively. For LIM and AFM, unstained preparations were used.

For LIM measurements, a MIA-1 microscope (VNIIOFI, Russia) was used. The principle of the method and the relevant equipment have been described in detail in previous works [7, 8].

AFM images were obtained using the NTEGRA SPECTRA (NT-MTD, Zelenograd, Russia) complex and the NOVA (NT-MDT) software package. The measurements were performed in the semi-contact mode using an NSG 10-A cantilever with the mean elastic modulus of 11.8 N/m and average curvature radius 10 nm. The scanning area was 40 × 40 μm (256 × 256 pixels) and the scanning frequency was 1 Hz. AFM and LIM images were processed with the SPIP 6.0 (Image Metrology A/S, Hørsholm, Denmark) software package. To determine the lateral dimensions of the objects in phase images, Fourier analysis of averaged image profiles was applied, with particle size determined by the characteristic frequencies in the Fourier spectrum. The smoothness (*S*) parameter in AFM and LIM images was calculated from the formula:

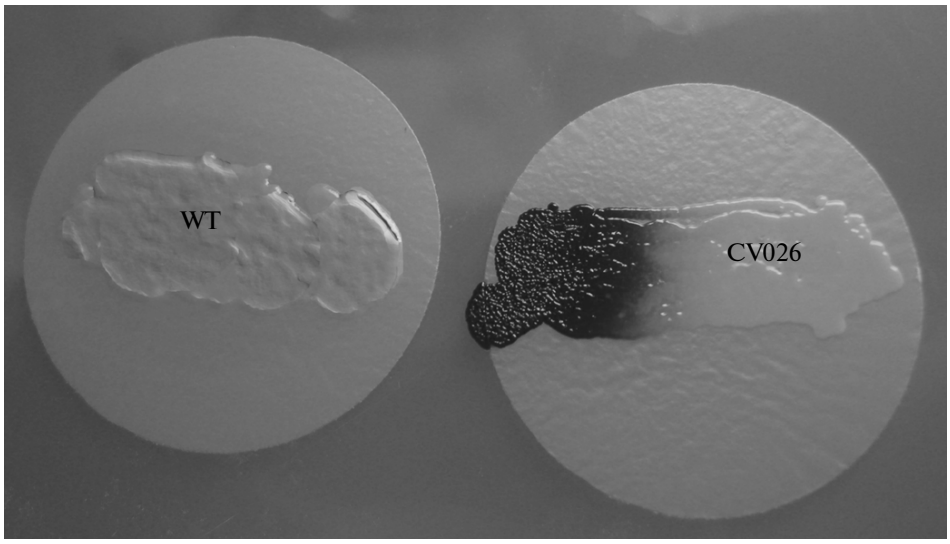

Fig. 1. Restoration of the ability to form violacein in the mutant *C. violaceum* CV026 in the presence of *C. violaceum* WT (polycarbonate filters upon LB agar).

$$S = \frac{1}{MN}\sum_{k=0}^{M-1}\sum_{l=0}^{N-1}|z(x_k, y_l)|, \quad (1)$$

where MN is a pixel number in the x and y coordinates, respectively, k and l are pixel indexes, and z is an amplitude of the x_k, y_l pixel.

Range of heights (S_z) in AFM images was calculated as the difference between the lowest and the highest pixel in the image.

$$S_z = z_{\max} - z_{\min}. \quad (2)$$

Fractal dimensions (S_{fd}) in AFM images were calculated using the algorithm implemented in the SPIP 6.0 software.

Electron microscopy was carried out on a JEM-100C (Jeol, Japan) microscope using the standard methods of negative staining and ultrathin sections. The biofilm preparations were transferred onto Formvar-covered copper grids (Serva, Heidelberg, Germany) and stained with 2% phosphotungstic acid (pH 3.5). Ultrathin sections were obtained with an LKB-3R microtome and stained with 3% uranyl acetate aqueous solution. The preparations were viewed in the microscope at 7000–20000× magnification.

Light microscopy. A characteristic feature of the *C. violaceum* mutant CV026 is its inability to synthesize a violet pigment violacein in the absence of exogenous acyl homoserine lactones. Introduction of *N*-butanoyl, *N*-hexanoyl, or *N*-octanoyl homoserine lactones into the medium restores the wild type phenotype, as may be seen from the development of violet coloration of the mutant cells. A similar effect is produced by the presence of a pigment-free (not capable of violacein synthesis) strain WT, which is capable of excretion of *N*-hexanoyl homoserine lactone into the medium. The effect of acyl homoserine lactones produced by strain WT and diffusing into the medium on the CV026 mutant cultured on LB agar is presented on Fig. 1.

Figure 2 shows typical images of the biofilms of *C. violaceum* WT and its mutant CV026 obtained by PCM after staining with DMMB.

It can be seen that, in accordance with our earlier hypothesis [1], the biofilm of the mutant was characterized by lower content of the matrix components, so that "naked" (not immersed into the matrix) cells and microcolonies predominated (Fig. 2b). It may be assumed that individual oval inclusions of matrix are caused by local reversions of the mutant to the wild type with the restoration of matrix synthesis. However, this assumption requires further studies.

In the area of action of *N*-acyl homoserine lactones diffusing through the medium, activation of violacein biosynthesis (Fig. 1) was observed, together with accumulation of the DMMB-stained matrix components (Fig. 2d). Violacein was found only in the cells and did not stain the matrix.

Unlike the standard PCM, the LIM technique provides for quantitative assessment of optical path difference (OPD), which in turn allows for considerable broadening and automation of image analysis. Using LIM, phase images of OPD distribution are for at each point of an object. Particulars of LIM application to various microbiological objects are reported in [7]. The value measured by OPD in each point of an object plain is a sum of products of refraction index and

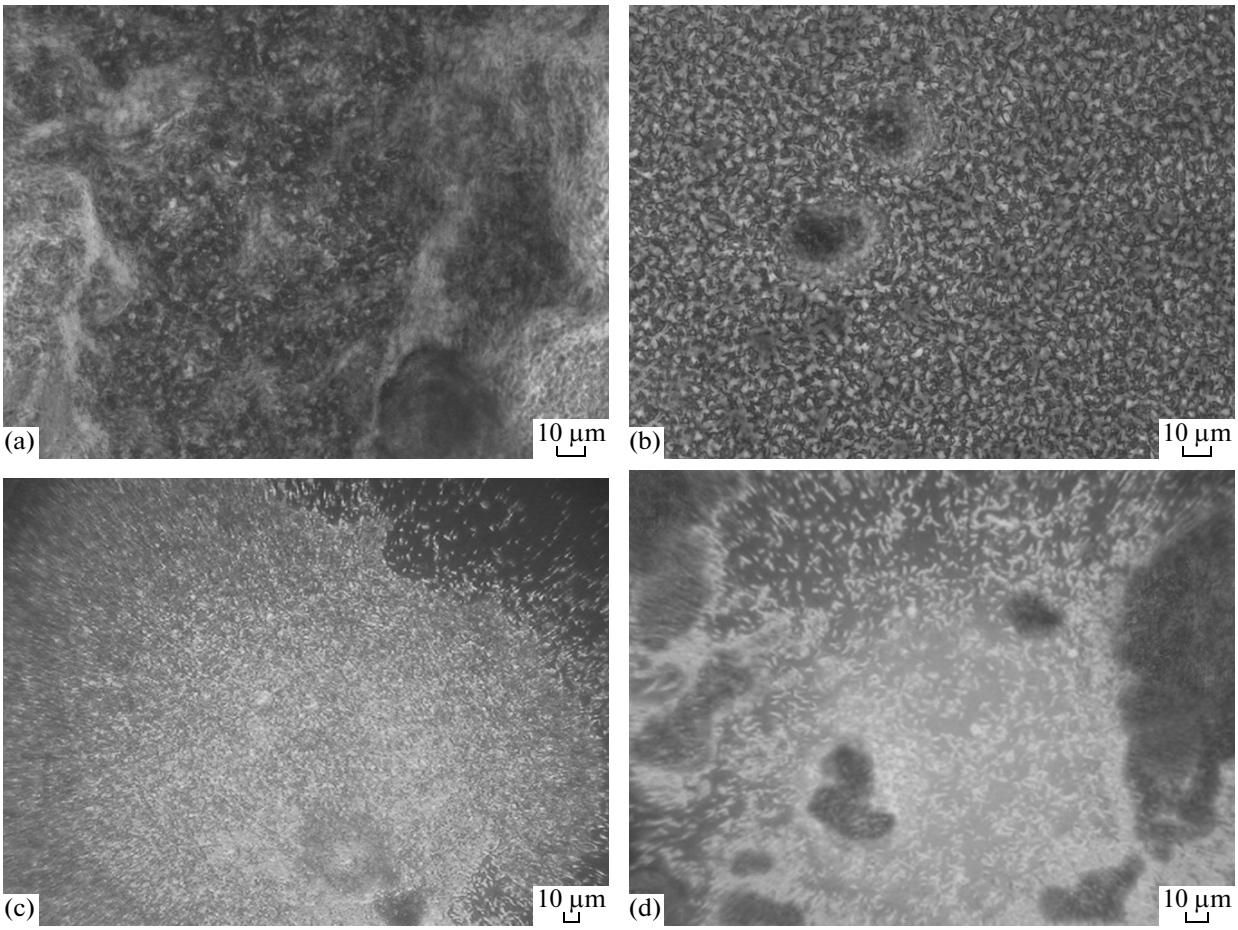

Fig. 2. PCM of biofilms (grown on cover slips) after DMMB staining: *C. violaceum* WT (a); CV026 mutant in the absence of *N*-acyl homoserine lactones in the medium (b); biofilms of the CV026 mutant grown on filters (see Fig. 1): sample collected from the zone containing no violacein (c) and sample collected at the edge of the zone containing violacein (d).

thickness of various optical media (cultivation medium, cells, etc.) at that point [8]:

$$\mathrm{OPD} = \left(n_1 z_1 + n_2 z_2 + \ldots + n_n z_n\right) - n_m z, \qquad (3)$$

where z and n are the thickness and refraction index of an optical medium, respectively.

Therefore, phase images of the biofilms may be interpreted as two-dimensional projections of the three-dimensional biofilm structure, while unevenness of the objects may result either from the geometry of biofilms (relief roughness) or, more likely, from the differences in the biofilm structure (for example, higher refractive index of the cells or the presence of cavities).

Typical phase images of WT and CV026 biofilms are presented on Fig. 3.

The difference in the OPD value was on average 9 times higher in the WT strain than in CV026, which was probably determined by the differences in thickness of the biofilms under study. To analyze the images, it seems most reasonable to estimate the lateral dimensions of the objects, average sample thickness, and roughness of the objects (as it is accepted, for example, in material science for evaluation of the characteristics of films). Typical dimensions for strains WT and CV026 are presented in Table 1.

Lateral dimensions of the objects measured with LIM were in the range of 10–15 μm, thus considerably exceeding the size of a single bacterium, and rather corresponded in size to bacterial microcolonies. The internal structures determined by LIM were most probably microcolonies, i.e., compact cell aggregates in the matrix.

While the roughness (variations in height with respect to the average value) differed for CV026 and WT, the difference was most likely due to the initial thickness of the films (the thicker the film, the rougher it is).

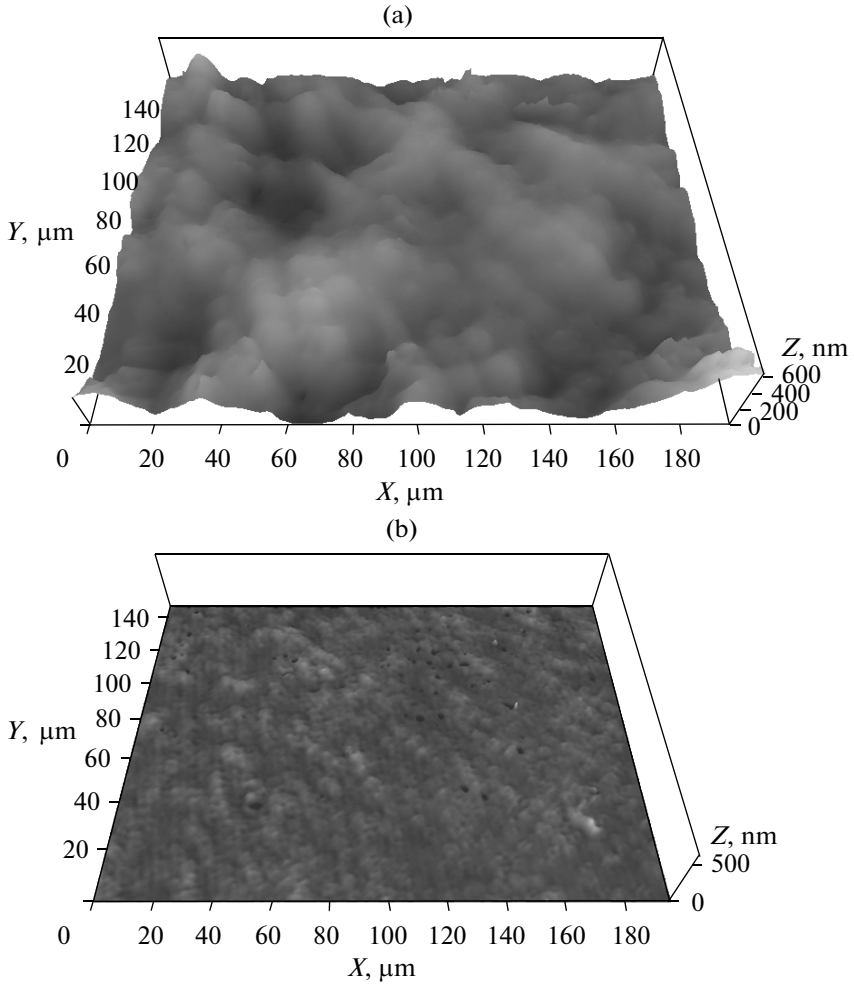

Fig. 3. Typical phase images of the biofilms formed by *C. violaceum* WT (a) and *C. violaceum* CV026 mutant (b).

Greater values of roughness and average thickness of the samples in the case of WT were caused by the higher matrix content inside the biofilm of this strain.

Considerable differences in the biofilm structure and matrix content were confirmed by epifluorescence microscopy (Fig. 4).

Table 1. Smoothness of the biofilms formed by *C. violaceum* strains

Strains	Typical lateral dimensions of the objects, μm	Average thickness (OPD), nm	Smoothness, nm
WT	19.7 ± 2.0	284.5 ± 63.6	288.7 ± 62.2
CV026	14.7 ± 1.5	30.1 ± 8.5*	40.6 ± 18.2*

Note: The data are presented as average values ± standard error ($n = 10$).
* $P < 0.05$, Student's criterion for independent sets.

To reveal the matrix, high concentration of DAPI (100 μg/mL) and prolonged staining (up to 30 min) were used, according to recommendations in [6]. Under these conditions, DAPI accumulates in the matrix and visualizes it due to its inherent fluorescence. Fluorescence of the cells immersed in the matrix is shielded.

Electron microscopy. Since the matrix components are dissolved in the process of sample preparation for transmission electron microscopy, typical electron microscopy images were unsuitable for reliable detection of the differences between the strains (Figs. 5a and 5b). However, contrasting with phosphotungstic acid preserved some of the matrix components, namely, the membrane vesicles (MV) tightly associated with microbial cells (Fig. 5a), which are common components of many microbial biofilms. These structures were present in abundance in the biofilms of *C. violaceum* WT and were practically absent from the preparation of the CV026 mutant.

The presence of MVs in the biofilm matrix of gram-negative bacteria and their probable role are discussed in detail in a number of studies. The internal contents of the MV vary, depending on the physiological state of the biofilm-forming microorganism, and may include a number of periplasmic components: proteinases, lipases, alkaline phosphatase, autolysins, and toxins. MVs are also the major source of lipopolysaccharides in the biofilm matrix [9]. In the case of *Helicobacter pylori*, MVs were shown to be directly involved in biofilm formation, providing for the adhesion of the cells to each other and to the phase boundary [10]. The complexes formed by MVs with free DNA present in the matrix may affect the biofilm surface properties [11].

Atomic force microscopy. Surface structures of the biofilms formed by *C. violaceum* WT and its mutant CV026 were studied by AFM (Fig. 6).

As can be seen from the figure, *C. violaceum* WT biofilm had a well-developed matrix with individual cells immersed in it, while in the preparation of the mutant *C. violaceum* CV026 the matrix was practically absent and the cells lay directly on the support.

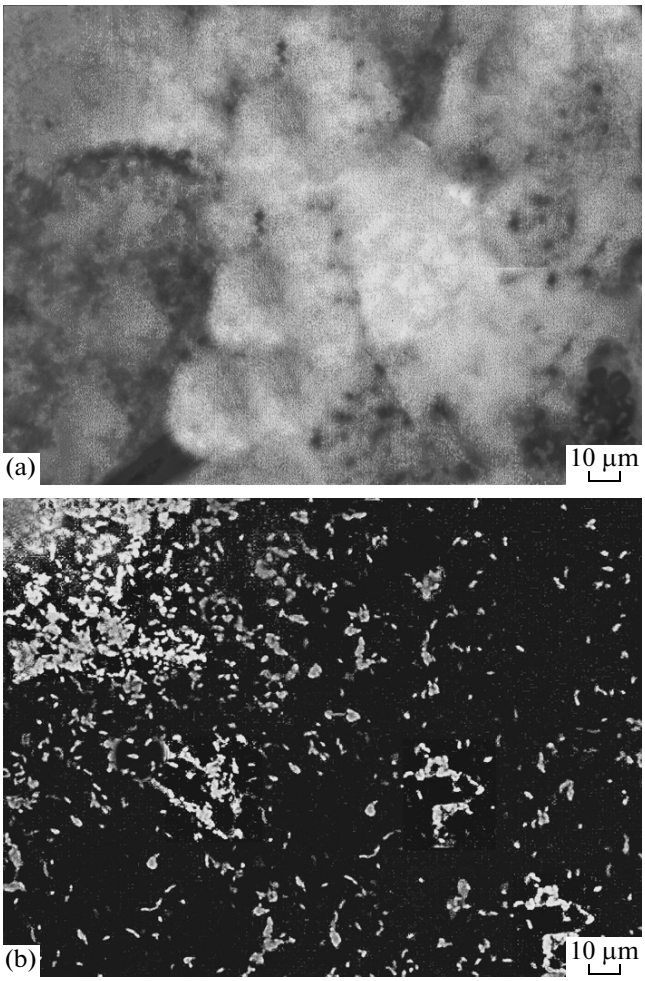

Fig. 4. Epifluorescence microscopy of DAPI-stained biofilm preparations. Biofilms of *C. violaceum* WT (a) and *C. violaceum* mutant CV026 (b).

Table 2. Characteristics of the surfaces of the biofilms formed by *C. violaceum* WT and *C. violaceum* CV026 mutant

Characteristics	WT	CV026
Sa, nm, smoothness parameter	244 ± 20	87 ± 2*
Sz, nm, height range	1680 ± 72	639 ± 32*
Sfd, nm, fractal dimension	2.843 ± 0.009	2.697 ± 0.004*

Note: The data are presented as average values ± standard error ($n = 10$).
* $P < 0.05$, Student's criterion for independent sets.

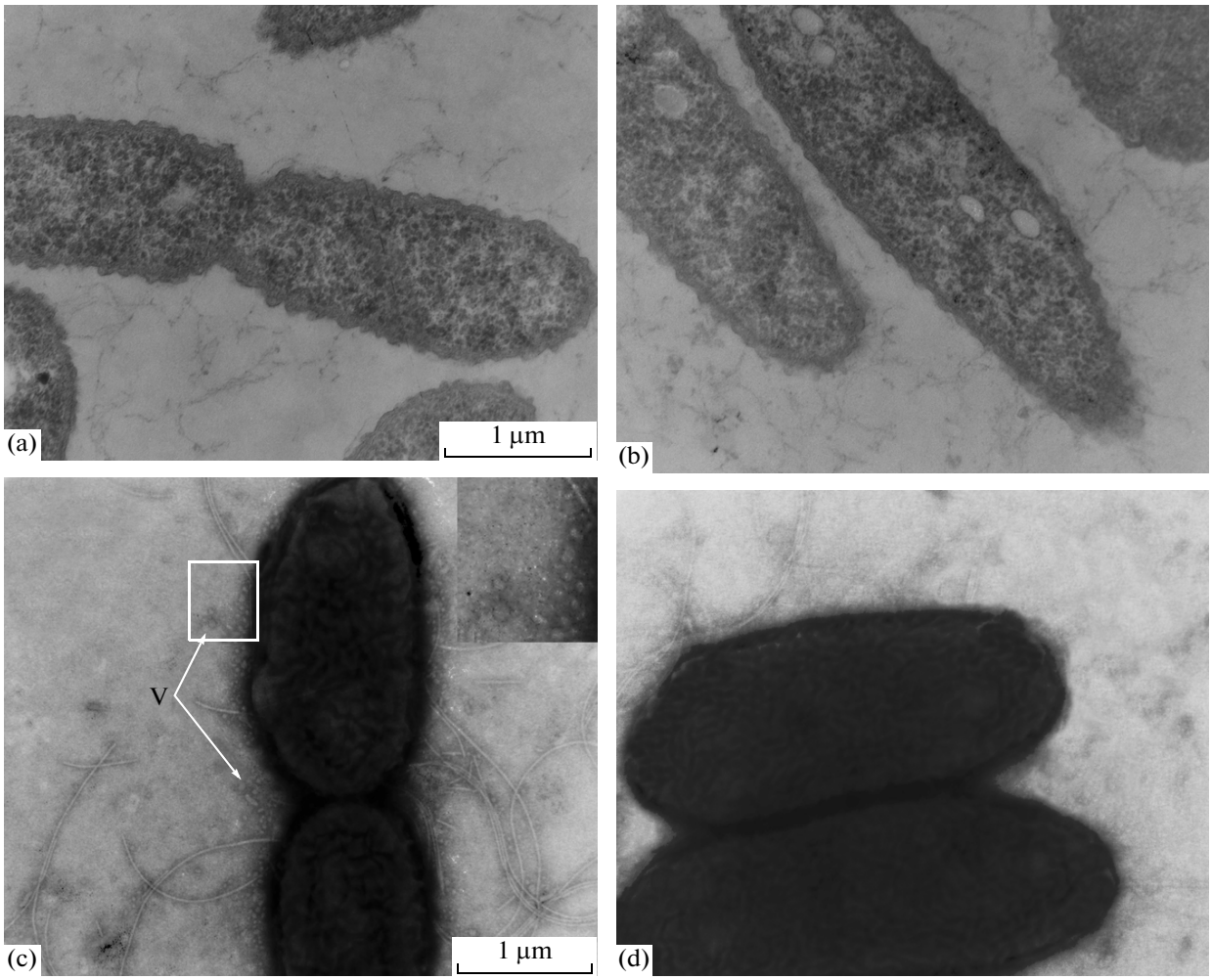

Fig. 5. Ultrathin sections of the biofilms of *C. violaceum* WT (a) and *C. violaceum* CV026 mutant (b). Biofilms of *C. violaceum* WT (c) and *C. violaceum* CV026 mutant (d) contrasted with phosphotungstic acid. V, membrane vesicles. Large-scale image of the indicated fragment is presented in the cut-in (the images are inverted).

The obtained AFM images provided for quantitative characterization of the biofilm surface relief. The parameters of smoothness, range of heights, and fractal dimensions for the biofilms of two strains were calculated (Table 2). The surface of *C. violaceum* WT biofilm was reliably rougher, with larger values of height range and fractal dimensions. These differences reflected the presence of a larger amount of unequally distributed components of the matrix in *C. violaceum* WT biofilm.

Average optical path difference (OPD) is related to the biofilm thickness, and roughness is probably caused by internal structure, reflecting not only the differences in the film thickness, but also different refraction indices of the biofilm substance (different concentration or nature of substances).

Therefore, staining of the biofilm matrix with a specific dye made it possible to detect the differences in the process of matrix accumulation using rather simple methods of PCM and EpiFM. Application of LIM and AFM, used to characterize the surfaces, provided the opportunity not only to visualize the biofilm matrix, but also to characterize quantitatively some peculiarities of its structure.

The results obtained completely support our earlier conclusion that the defects in the quorum sensing regulatory system in the mutant strain *C. violaceum* CV026 manifest themselves as characteristic features in the biofilm matrix formation, which correlates with its increased sensitivity to environmental physicochemical factors [1]. According to our preliminary data, the biofilm of this mutant strain is characterized by low resistance to a number of antibacterial antibiotics, which agrees with the concept of the barrier func-

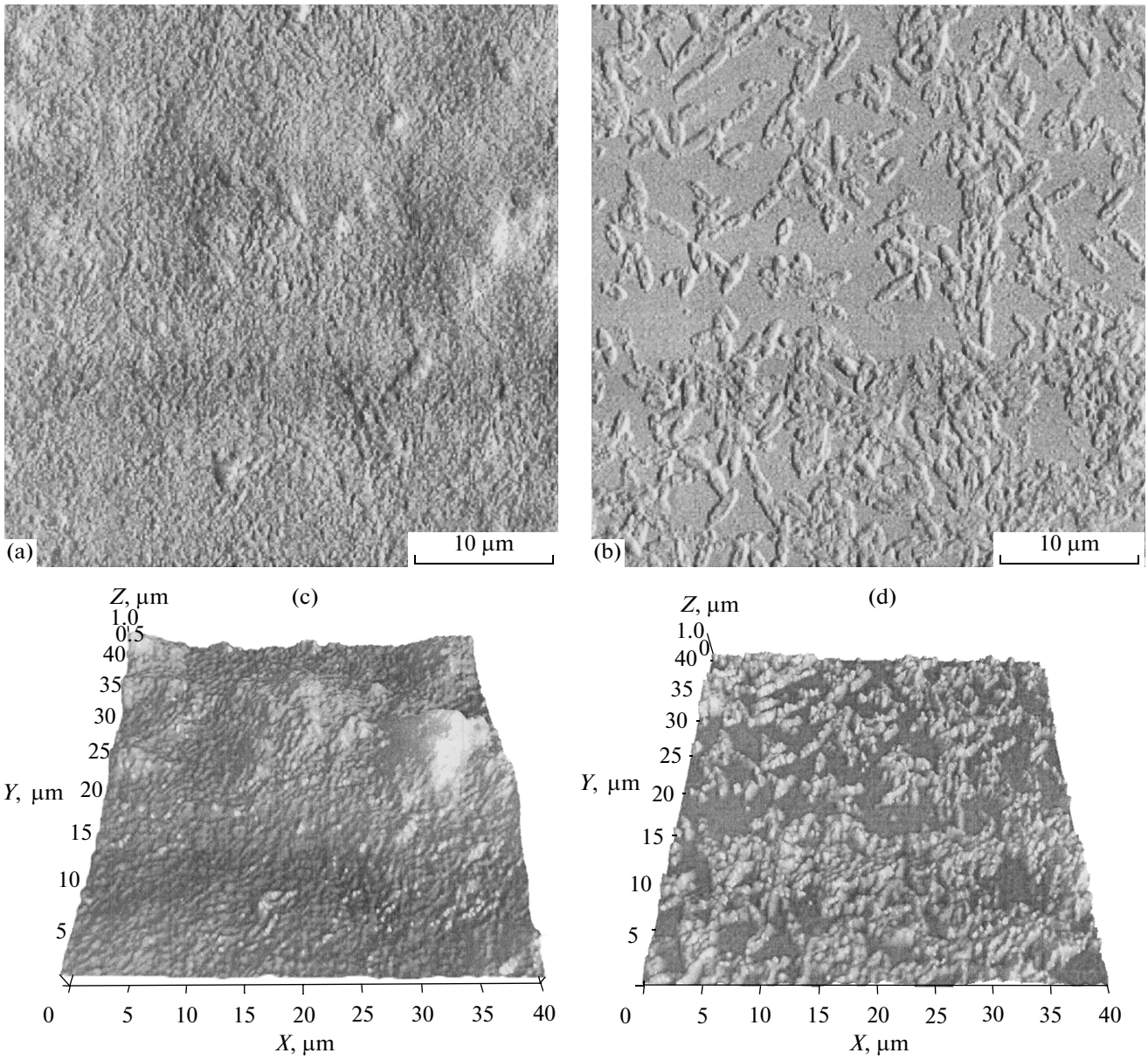

Fig. 6. AFM images of the biofilms of *C. violaceum* WT (a), (c) and *C. violaceum* CV026 mutant (b), (d). The images were obtained by methods of disalignment (a), (b) and quasi-three-dimensional distribution of heights (c), (d).

tion of complete (mature) matrix of biofilms with respect to these biocides [12].

REFERENCES

1. Strelkova, E.A., Pozdnyakova, N.V., Zhurina, M.V., Plakunov, V.K., and Belyaev, S.S., Role of the extracellular polymer matrix in resistance of bacterial biofilms to extreme environmental factors, *Microbiology*, 2013, vol. 82, no. 2, pp. 119–125.
2. McClean, K.H., Winson, M.K., Fish, L., Taylor, A., Chhabra, S.R., Camara, M., Daykin, M., Lamb, J.H., Swift, S., Bycroft, B.W., Stewart, G.S.A.B., and Williams, P., Quorum sensing and *Chromobacterium violaceum:* exploitation of violacein production and inhibition for the detection of *N*-acylhomoserine lactones, *Microbiology* (UK), 1997, vol. 143, pp. 3703–3711.
3. Peeters, E., Nelis, H.J., and Coenye, T., Comparison of multiple methods for quantification of microbial biofilms grown in microtiter plates, *J. Microbiol. Meth.*, 2008, vol. 72, pp. 157–165.
4. Romling, U., Sierralta, W.D., Eriksson, K., and Normark, S., Multicellular and aggregative behaviour of *Salmonella typhimurium* strains is controlled by mutations in the *agfd* promoter, *Mol. Microbiol.*, 1998, vol. 28, pp. 249–264.
5. Stepanova, T.V., Romanova, Yu.M., Alekseeva, N.V., Navol'nev, S.O., Navol'neva, O.S., and Gintsburg, A.L., Development of anti-biofilm agents: Investigation of the action of polysaccharide lyases on the

matrix of the *Pseudomonas aeruginosa* and *Burkholderia cenocepacia* biofilms, *Med. Alfavit. Sovr. Labor.*, 2010, no. 1, pp. 47–51.

6. Azevedo, N.F., Pacheco, A.P., Keevil, C.W., and Vieira, M.J., Adhesion of water stressed *Helicobacter pylori* to abiotic surfaces, *J. Appl. Microbiol.*, 2006, vol. 101, pp. 718–724.
7. Yusipovich, A.I., Berestovskaya, Yu.Yu., Shutova, V.V., Levin, G.G., Gerasimenko, L.M., Maksimov, G.V., and Rubin, A.B., New possibilities of studying microbial objects by laser interference microscopy, *Biophysics*, 2011, vol. 56, pp. 1063–1068.
8. Yusipovich, A.I., Zagubizhenko, M.V., Levin, G.G., Platonova, A., Parshina, E.Yu., Grygorzcyk, R., Maksimov, G.V., Rubin, A.B., and Orlov, S.N., Laser interference microscopy of amphibian erythrocytes: Impact of cell volume and refractive index, *J. Microscop.*, 2011, vol. 244, pp. 223–229.
9. Schooling, S.R. and Beveridge, T.J., Membrane vesicles: An overlooked component of the matrices of biofilms, *J. Bacteriol.*, 2006, vol. 188, pp. 5945–5957.
10. Yonezawa, H., Osaki, T., Kurata, S., Fukuda, M., Kawakami, H., Ochiai, K., Hanawa, T., and Kamiya, S., Outer membrane vesicles of *Helicobacter pylori* TK1402 are involved in biofilm formation, *BMC Microbiol.*, 2009, vol. 9, pp. 1–12.
11. Schooling, S.R., Hubley, A., and Beveridge, T.J., Interactions of DNA with biofilm-derived membrane vesicles, *J. Bacteriol.*, 2009, vol. 191, pp. 4097–4102.
12. Strelkova, E.A., Zhurina, M.V., Plakunov, V.K., and Belyaev, S.S., Stimulation of biofilm formation by antibiotics, *Microbiology*, 2012, vol. 81, no. 2, pp. 259–262.

Translated by N. Kuznetsova